aerospace

MDPI

Article

Simulation and Test of Discrete Mobile Surfaces for a RC-Aircraft

Francesco Nicassio † **and Gennaro Scarselli** *,†

Department of Engineering for Innovation, University of Salento, Via per Monteroni, 73100 Lecce, Italy; francesco.nicassio@unisalento.it

* Correspondence: gennaro.scarselli@unisalento.it; Tel.: +39-0832-299720

† These authors contributed equally to this work.

Received: 10 June 2019; Accepted: 1 November 2019; Published: 5 November 2019

Abstract: Morphing structures suitable for unmanned aerial vehicles (UAVs) have been investigated for several years. This paper presents a novel lightweight, morphing concept based on the exploitation of the "lever effect" of a bistable composite plate that can be integrated in an UAV horizontal tail. Flight dynamics equations are solved in Simulink environment, thus being able to simulate and compare different flight conditions with conventional and bistable command surfaces. Subsequently, bistable plates are built by using composite materials, paying particular attention to dimensions, asymmetric stacking sequence and total thickness needed to achieve bistability. NACA0011 airfoil is chosen for proving this concept. Wind tunnel tests demonstrate that the discrete surface is capable of withstanding the aerodynamic pressure. A remotely piloted vehicle is employed to test the discrete horizontal tail command during the take-off. The results show that, choosing a proper configuration of constraints, stacking sequence and aspect ratio for the bistable laminate, it is possible to tailor the snap-through mechanism. The proposed concept appears lighter and increases aerodynamic efficiency when compared to conventional UAV command surfaces.

Keywords: morphing surfaces; bistable materials; RC-UAV

1. Introduction

Unmanned aerial vehicles (UAVs) may operate with various degrees of autonomy: either under remote control (RC) by a human operator or autonomously by on-board computers [1–3]. Compared to manned aircraft, UAVs were originally used for missions dull, dirty or dangerous and they can operate in environments contaminated by chemical, biological or radioactive agents. While they originally fitted mostly military applications, now their use is rapidly expanding to commercial, scientific, agricultural, recreational and other civil applications [4–8]. For this reason, in recent years there has been an increasing interest for (i) lighter-than-air UAVs with significantly higher endurance that can be used for persistent area surveillance [9]; (ii) long–endurance UAVs that can fly for several days [10–12] and (iii) small UAVs that are versatile, portable and easy to maintain [13,14].

In addition to these applications, UAVs provide an ideal platform for exploring and developing innovative solutions in the aeronautical engineering since the risk level is acceptable at this scale, and they have more manageable fabrication and less operational costs [15]. One example of this is the emergent idea of a morphing concept applied to aircraft lifting surfaces, which is the focus of this work. On this topic, several alternatives are reported in the technical literature, in terms not only of materials and structural parameters but also of feasibility and efficiency of the proposed solutions [16]. De Breuker and Werter in [17] demonstrated the strong influence of the aircraft speed on the maximum values of actuation forces in a morphing mechanism as well as the importance of the order in which various morphing deformations are executed. An adaptive trailing edge concept

was presented in [18] by combining conventional parts and innovative concepts, as the morphing skin assembled into a new structural system: an outboard wing trailing edge, consisting of three articulated (finger-like) rib covered by a multi–material hyperelastic skin. In [19] the antagonistic shape memory alloys (SMA) were used for wing morphing of small RC UAVs reducing the weight due to the actuation systems. Pecora et al. in [20,21] studied the design assessment of an innovative flap architecture for a variable-camber trailing edge: the reference geometry was based on a wing, where the conventional flap component was replaced by a morphing trailing edge based on compliant ribs.

Among the morphing solutions proposed in last years, in terms of materials able to withstand aerodynamic loads, multistable materials were investigated for UAV morphing concepts: multistability is the property of varying geometrical shape with only small energy input and structures having this attribute represent an interesting candidate for the development of morphing solutions. Nicassio et al. in [22] explored bistable plates dynamic behavior for designing novel morphing command surfaces. In order to improve the UAVs aerodynamic performances, in [23] a prototype of morphing winglet utilizing a metallic bistable structure and polymer was presented. The metallic bistable structure was manufactured by bending a metal sheet and had two stable shapes: one was flat and the other was curved. To obtain an airfoil shape, the metallic bistable structure was placed in a mold with the shape of the airfoil and the polymer was poured into the mold for keeping the shape. The main finding of [24] is that multistable winglets are effective (especially at large dynamic pressure and angles of attack (AOAs)) in controlling the lateral and directional stability, but their efficiency in the lateral control, especially at low dynamic pressures, strongly diminishes respect to conventional ailerons. In addition, since their operational capabilities are strongly affected by the AOA, they can suffer roll reversal phenomena when wing's AOAs are negative. Wang in [25] demonstrated that a morphing bistable composite structure could be produced, based on the principles of viscoelastically generated prestress: a composite plate structure was created in order to snap into one of two cylindrical states. In [26] guidelines were proposed to design a morphing unsymmetric panel/actuator assembly, while in [15] a passive mobile surface with a bistable plate was presented. In the latter paper, the bistable morphing surface was activated using a proper configuration of constraints. These ad-hoc boundary conditions allowed the snap-though with activating forces of magnitude comparable with the differential pressure around a typical aeronautical airfoil. The possible applications of such behavior were the bistable composite integration in a low energy passive mobile surface able to autonomously react to pressure variations with a lift reduction when a maximum altitude was reached and vice versa.

In the present manuscript a novel horizontal stabilizer concept for small RC-UAV (illustrated in the schematic of Figure 1) is designed by using composite bistable plates on which, in the future, micro fiber composite (MFC) will be applied and used as actuators. The main goals of this work are to (i) enhance the aerodynamic efficiency of the UAV control surfaces through the activation system integrated in the wing/tail box, (ii) replace the conventional UAV mechanical flight control system with an electronic one, with a resulting weight reduction, (iii) reduce the energy/load requirement since this system does not require transducers or servo-actuators to maintain the stable shapes but just to activate the snap-through.

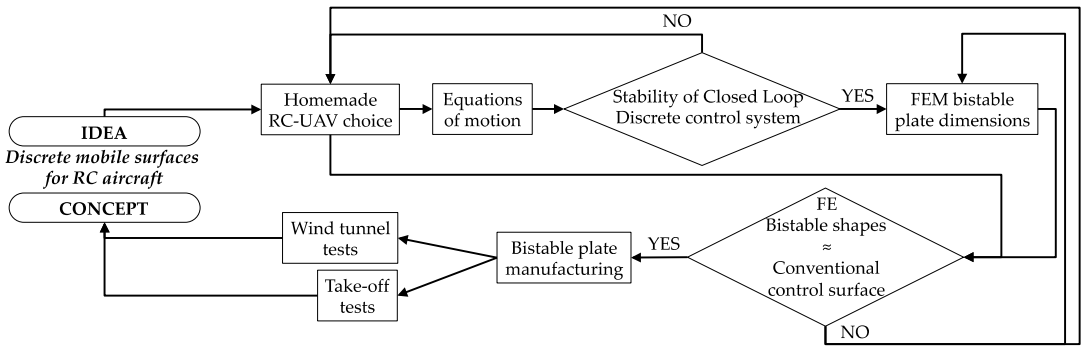

Figure 1. Schematic of the present research.

The main advantages of this proposed concept are the following: the concept based on the activation of bistable is mechanically much simpler than the conventional mechanisms needed for the control of the mobile surfaces, consisting in command lines, pulleys, hinges and so on; one direct consequence of the simplicity is that also the inspection and maintenance are relatively easier for the bistable command system than the conventional one; in addition, the energy/load requested by the proposed solution is also lower than the one requested by the common kinematic chains, since in the latter the deflection of the mobile surface must be kept by an external reaction force able to withstand the aerodynamic pressure while in the former the deflection of the mobile surface is kept by an internal reaction force due to the thermal residual stresses inside the bistables.

The present manuscript is not intended to cover all the design aspects typical of an aeronautical part even simple like the control surface of a small UAV. The activities hereinafter reported are a preliminary investigation about the technical feasibility of a control surface based on the employment of bistable materials. As such, the following research questions are addressed and answered: is it possible to control the flight of a typical UAV relying on a control surface capable only of discrete displacements? Can a bistable plate mimicking the conventional control surface with a reasonable weight and cost be designed and manufactured? Can such a plate actually be integrated into an aeronautical base profile?

Following the choice of the UAV benchmark, the flight dynamics equations are implemented in MATLAB (Version R2015, The MathWorks, Inc., Natick, MA, USA) and Simulink environment in order to simulate different flight conditions (e.g., open and closed loop simulation, gust response and take-off maneuver). After checking the stability of closed loop bistable control system, the analytical results, in terms of discrete displacement of mobile surfaces to reach specific mission goals (i.e., elevator, ailerons and rudder), are used for the finite element (FE) simulations as design requirements (how much the bistable plate must deform). By using appropriate boundary conditions, it is demonstrated that the bistable shapes can be tailored to match these requirements. From the results of the FE analyses, carbon fiber reinforced polymers (CFRPs) plates were manufactured with aspect ratio (AR), total thickness, dimensions and asymmetric stacking sequence previously simulated in order to achieve the bistability. In the next step, wind tunnel tests are carried out in order to prove that the bistable system (integrated in a wing sample with the same UAV airfoil) remains in one of two stable geometries during the test and both the states are able to withstand the aerodynamic loads without any additional holding forces or locking mechanisms. Eventually, the discrete mobile surface behavior is validated by real flight tests. At this stage of the investigation using a conventional mobile surface in the "discrete mode" (just two possible deflections) is the only possible experiment. Following the experiments, the numerical model is furthermore validated matching the experimental take-off lengths with the numerical ones. The main finding is that the proposed innovative concept of bistable control surfaces actually works and the research can go to the next step: the implementation of an actual prototype of new horizontal stabilizer, by using bistable plates for the vehicle subject of study.

2. Models, Materials and Methods

2.1. Flight Dynamics Equations and UAV Features

Under the hypotheses of flight in calm air, the motion equations valid for the UAV subject of investigation in the present study [27] can be expressed in an inertial frame and projected over a set of body-axes (see Figure 2).

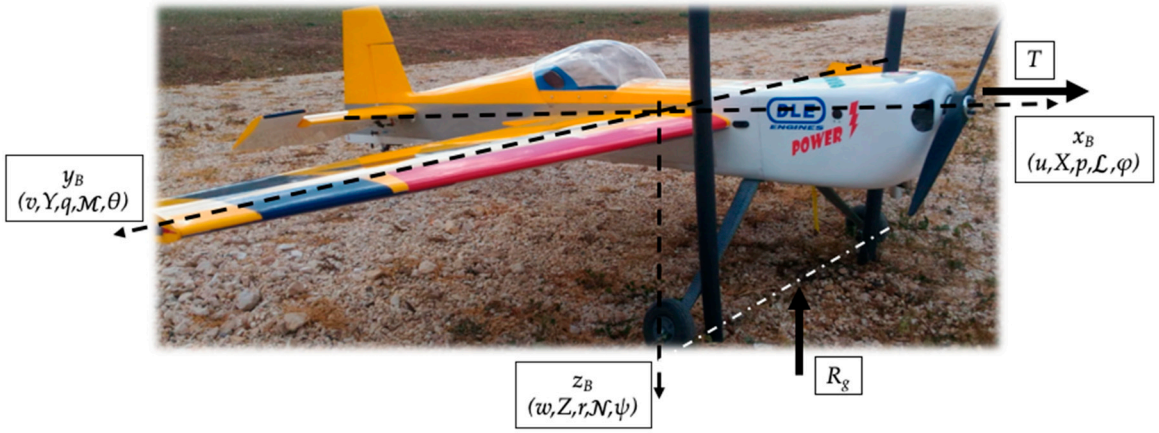

Figure 2. Unmanned aerial vehicle (UAV) body axes (x_B,y_B,z_B) with: (u,v,w) velocities of the UAV centre of mass; (X,Y,Z) aerodynamic forces; (p,q,r) angular speeds; ($\mathcal{L}$, $\mathcal{M}$, $\mathcal{N}$) roll, pitch and yaw aerodynamic moments, (φ,θ,ψ) roll, pitch and yaw angles; T thrust; R_g ground reaction; m mass.

They form a system of 12 first order nonlinear ordinary differential equations (ODEs):

- Dynamics of the centre of mass:

$$\begin{cases} \dot{u} + qw - rv = (X + T_x)/m - g\sin\theta \\ \dot{v} + ru - pw = \left(Y + T_y\right)/m + g\cos\theta\sin\phi \\ \dot{w} + pv - qu = (Z + T_z)/m + g\cos\theta\cos\phi - R_g \end{cases}. \tag{1}$$

- Attitude dynamics:

$$\begin{cases} I_x\dot{p} - I_{xz}\left(\dot{r} + pq\right) - \left(I_y - I_z\right)qr = \mathcal{L} \\ I_y\dot{q} - I_{xz}\left(r^2 - p^2\right) - (I_z - I_x)rp = \mathcal{M} \\ I_z\dot{r} - I_{xz}\left(\dot{p} - qr\right) - \left(I_x - I_y\right)pq = \mathcal{N} \end{cases}. \tag{2}$$

- Attitude kinematics:

$$\begin{cases} \dot{\phi} = p + q\sin\phi\tan\theta + r\cos\phi\tan\theta \\ \dot{\theta} = q\cos\phi - r\sin\phi \\ \dot{\psi} = q\sin\phi/\cos\theta + r\cos\phi/\cos\theta \end{cases}. \tag{3}$$

- Trajectory of the centre of mass:

$$\begin{cases} \dot{R}_N = u\cos\theta\cos\psi + v(\sin\phi\sin\theta\cos\psi - \cos\phi\sin\psi) + w(\cos\phi\sin\theta\cos\psi + \sin\phi\sin\psi) \\ \dot{R}_E = u\cos\theta\sin\psi + v(\sin\phi\sin\theta\sin\psi + \cos\phi\cos\psi) + w(\cos\phi\sin\theta\sin\psi - \sin\phi\cos\psi) \\ \dot{h} = -(-u\sin\theta + v\sin\phi\cos\theta + w\cos\phi\cos\theta). \end{cases} \tag{4}$$

In order to carry out the experimental campaign, a homemade RC UAV was selected. The choice of this UAV was based on the following reasons: it is simple to be managed; its basic main structure allows the future use of bistable surfaces; its aerodynamic behavior is easy to be simulated and many investigations on this type of aircraft are reported in the literature and research works; lastly the installed airfoil is widely used in mini UAV and small UAV, that represent the final application of this study. Geometric dimensions of the RC UAV are reported in Figure 3, mass, aerodynamic and thrust features in Table 1.

In order to verify the centre of mass position and to obtain the inertia moments of the actual UAV, a CAD model was developed using CATIA software (Version V5-6 R24 R2014, Dassault Systèmes SE, Vélizy-Villacoublay, France).

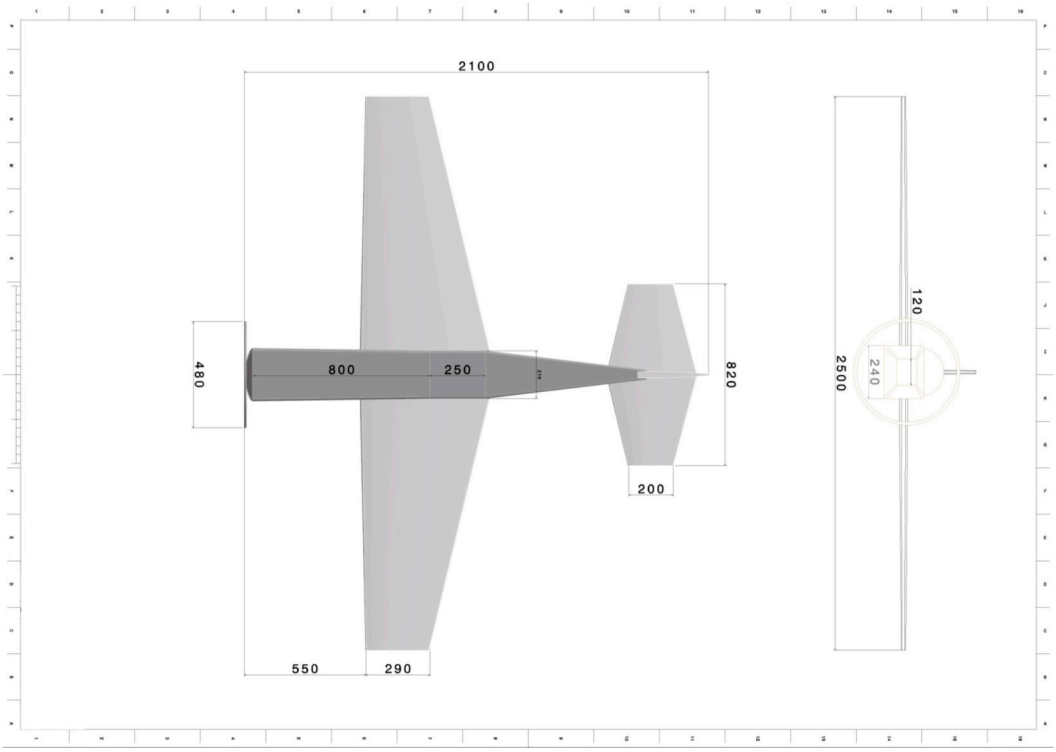

Figure 3. UAV geometric drawing, dimensions in millimeters.

Table 1. Unmanned aerial vehicle (UAV) main features.

Specification	Symbol	Value	Specification	Value
Mass and Inertia			**Aerodynamics**	
Mass	M	6.5 kg	Wing and Tail Profile	NACA 0011
UAV moment of inertia	I_x	0.681 kg m^2	**Thrust**	
	I_y	1.375 kg m^2	DLE Engine Power	5 CV
	I_z	2.0121 kg m^2	DLE Engine Displacement	30 cc
	I_{xy}	−0.001 kg m^2	Propeller Diameter	0.48 m
	I_{xz}	0.022 kg m^2	Propeller Pitch	0.30 m
	I_{yz}	0.0001 kg m^2	-	-

To evaluate the aerodynamic characteristics of the NACA0011 airfoil (wings, horizontal and vertical tail), XFOIL software [28] was used. This is an interactive program widely used for the design and analysis of subsonic isolated airfoils. The main airfoil characteristics are reported in Figure 4 and, according to the low speed considered in this work, Reynolds and Mach numbers were found to be equal to 400,000 and 0.04 respectively for all simulations.

The data in Figure 3, Table 1 and Figure 4 were used to perform in Simulink the following studies:

- Open-loop simulations by applying a specific command input to the elevator, ailerons and rudder: the command consisted in a 1 degree positive step;
- Closed-loop simulations (gust response by using Dryden wind turbulence model) with a full-state feedback control by means of the linear quadratic regulator (LQR) method;
- Take-off length simulations.

The last two simulations were carried out with both continuous and discrete operation modes of the mobile surface, to compare their effect on the UAV motion.

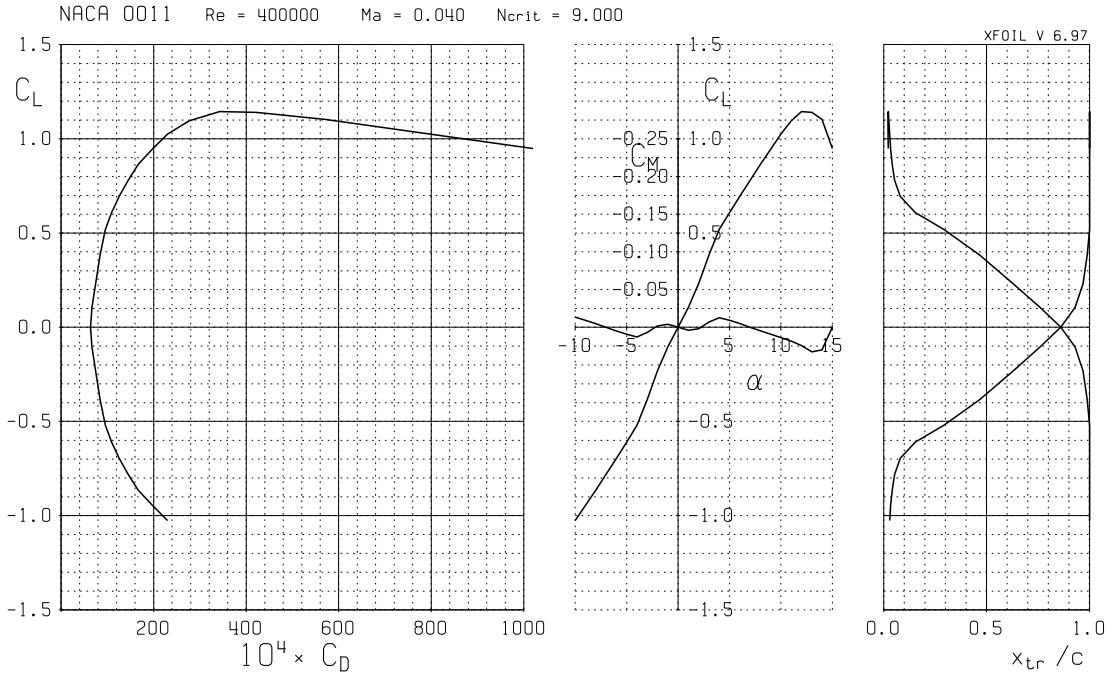

Figure 4. XFOIL aerodynamic properties of NACA0011.

2.2. FE Simulations and Manufacturing of Bistable Plates

A thermomechanical FE model [29] was developed to design the bistable composite plate as a morphing surface able to provide the same deflections of the continuous mobile surfaces. The entire analyses were split up in two load cases: the thermal simulation to induce the curved shapes and the transient simulation of the snap-through. The commercial software ANSYS® (Transient Structural Module, version 2019 R3, Ansys Inc., Canonsburg, PA, USA) was used [30]. To create the bistable stabilizer (for replacing the conventional one in Figure 2), a bistable rectangular plate with an AR of 2 (80 mm × 160 mm) was simulated by stacking four laminae following a $(0_2/90_2)$ sequence and exploiting the "lever effect" [15]: the leverage amplifies the input force to provide a bigger output effect. The ratio of the output force to the input is the mechanical advantage of the lever. This mechanism allows us to gain mechanical advantages by moving the septum, in terms of plate displacements and activation forces: to increase the displacement and decrease the activation load, the distance between the constrained edge and the septum must be as small as possible (see Figure 5a). The actual characteristic boundary conditions were carried out with one constrained edge and the adjustable septum (as in Figure 5b).

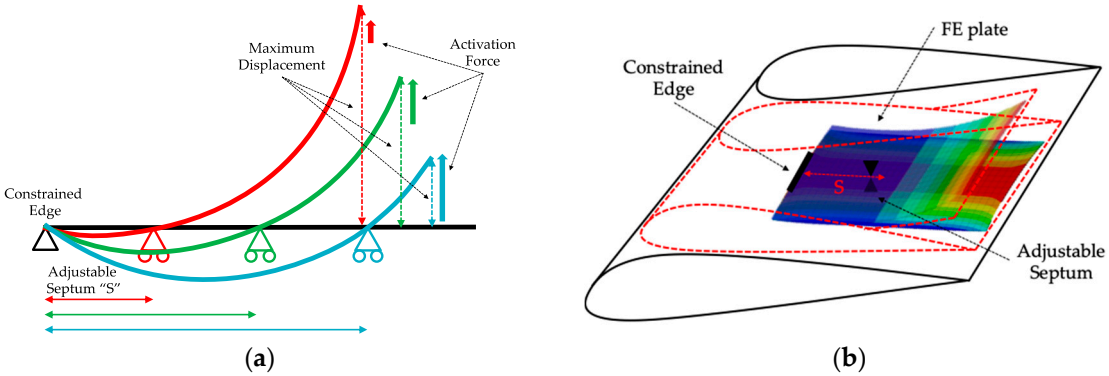

Figure 5. (**a**) Lever effect graphic and (**b**) finite element (FE) model (two stable states) on a UAV stabilizer.

The FE model consisted of shell elements. Convergence studies on the mesh size were carried out in order to achieve an acceptable accuracy of the results. The option "Large Deflection" was employed in each step because large deformations are associated with small displacement increments of the plate during the process (geometric non–linearity).

The available material was the prepregs Hexply 8552 with unidirectional carbon fibers IM7 (used in primary aerospace structures [31]). The main mechanical properties shown in Table 2 filled the engineering data module of the software for all simulations.

Table 2. Hexply 8552 data.

Technical Data	Value
Nominal cured ply thickness	0.131 mm
Nominal laminate density	1570 kg m^{-3}
Young's modulus 0° direction	165 GPa
Young's modulus 90° direction	11.4 GPa
Coefficient of thermal expansion 0° direction	6×10^{-7} C^{-1}
Coefficient of thermal expansion 90° direction	2.86×10^{-5} C^{-1}

The numerical results provided by FE models allowed us to know: (i) the displacements evaluated at the free end of the plate for different septum positions, (ii) the maximum deformations and (iii) the activation forces. The displacements values allowed us to evaluate the deflection capabilities of the discrete mobile surface. The knowledge of plate deformations was useful since it drives the choice of possible locations for a proper use of MFC P1/F1 actuators [32]: these actuators, in fact, bonded onto the plate and electrically activated, are deformed inducing the bistable snap-through. The activation forces intensity is strictly related to the amount of charge requested by the MFC.

In order to obtain experimentally the discrete shapes of bistable plates, four laminates with four layers of Hexply prepregs (see Figure 6) were manufactured.

(**a**) (**b**)

Figure 6. Bistable laminates manufacturing: (**a**) Hexply 8552 prepregs on the mold and (**b**) vacuum bag.

The samples were cured following the conventional cycle suggested by the manufacturer, setting the temperature at 180 °C, with the overall curing cycle of 3 h. In order to increase the thermal residual stresses and to obtain a higher level of curvature in the samples, the laminates, after the curing was completed in the autoclave, were immediately brought out so that a fast cooling down occurred in open air at room temperature. After the cooling down, each laminate was observed to have the two expected stable states (in Figure 7).

(**a**)

Figure 7. *Cont.*

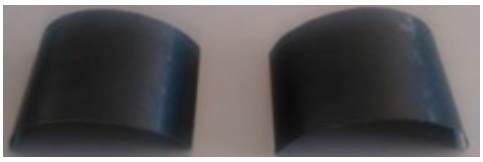

(**b**)

Figure 7. Experimental bistable plates: (**a**) first stable state and (**b**) second stable state.

3. Results and Discussion

3.1. Simulink Results

In this subsection the UAV response to input commands considered in the previous section was analyzed. The open-loop simulations were run to demonstrate that the Simulink model was effective. If a unit step is assigned to a mobile surface, its effect on the flight dynamics will be the same regardless if the command will be continuous or discrete. The closed-loop simulations instead provided information on how the control actions from the controller were dependent on the system dynamics. The closed-loop simulations were performed to make a comparison between continuous and discrete bistable command surfaces providing information useful to understand the technical feasibility of a discrete command.

3.1.1. Open-Loop Simulations

Unit step inputs after 1 s of trimmed flight were considered in all cases as inputs to the control mobile surfaces (initial trim conditions corresponding to an horizontal flight with speed and altitude equal to 10 m/s and 50 m respectively), in order to validate the Simulink model by means of flight mechanics equations.

Figure 8 represents the dynamic response in terms of motion variables to a positive (pitch-down) step input on the elevator. The first 20 s of simulation are reported, where it is possible to recognize the short–term response of short period variables, namely α and q. The AOA rapidly reaches a new equilibrium with well damped oscillations, whereas the pitch rate converges towards a small value. When a positive elevator step is applied, the initial force increment coming into play is directed upwards, and it causes a small but strictly positive increment to the flight-path angle. This causes the aircraft to enter an accelerating dive and u increasing.

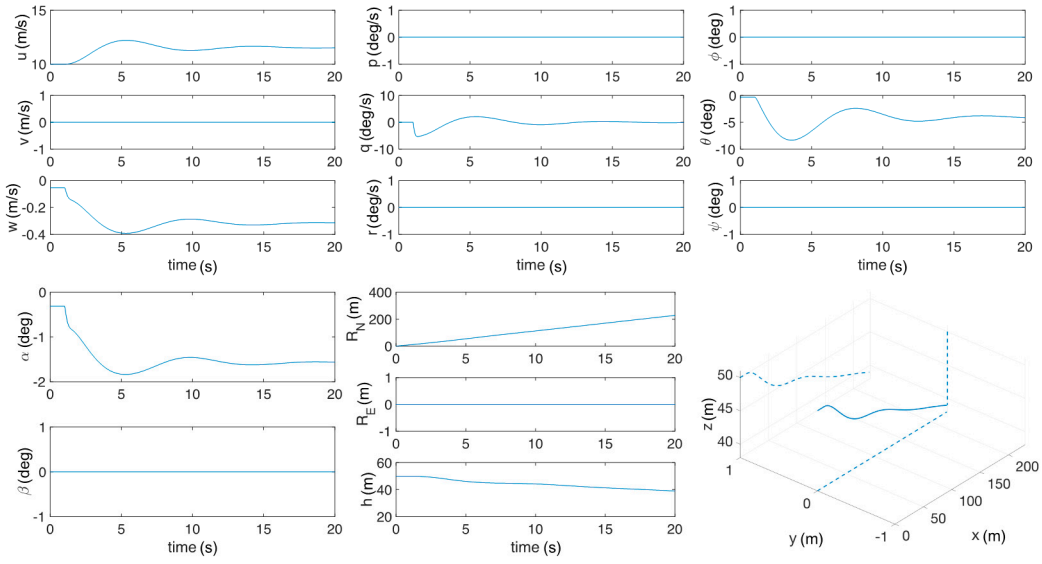

Figure 8. UAV response to the unit step elevator.

The response to a positive aileron step command was characterized by an initial transient (5–6 s) dominated by the roll mode, during which the UAV achieved a negative roll rate (Figure 9). The increment in the roll angle achieved during this phase caused the aircraft to sideslip (β became negative). A steady state yaw rate r was achieved for a constant roll angle φ, which means that the aircraft entered a steady turn. From the practical standpoint, it should be noted that the aileron control power in this case was related to the ailerons placed close to the root of the half-wing in order to limit the excitation of wing bending and torsional modes. This explains the small value of the roll rate p achieved in the maneuver.

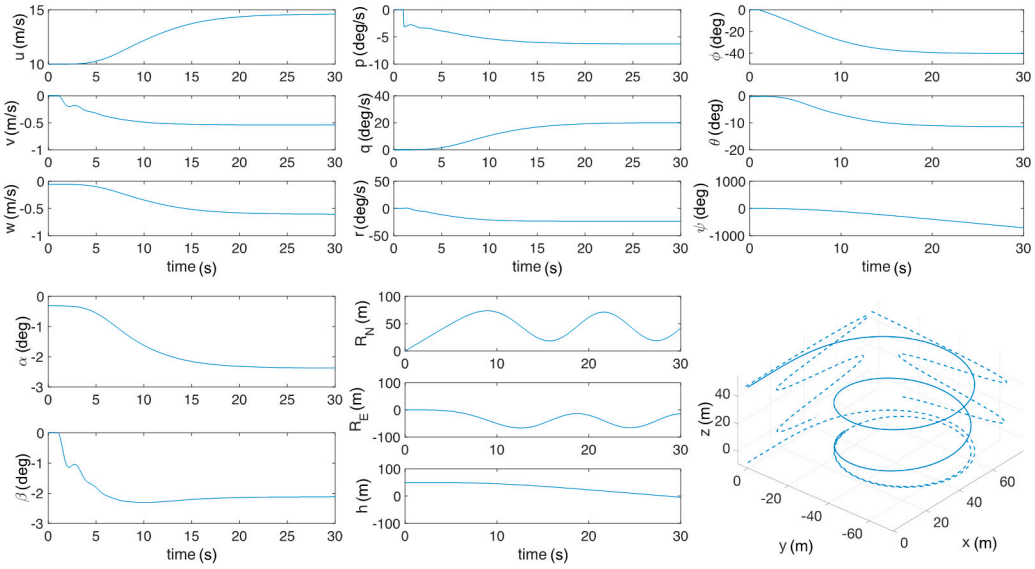

Figure 9. UAV response to unit step ailerons.

When a positive step command was applied to the rudder, the first effect was a linear acceleration around the yaw axis and the growth of the sideslip angle β, which became positive (Figure 10). The sideslip angle generated a negative rolling moment, thus inducing an increment of the roll angle φ, as achieved by the aileron command, but related to a different source. The response was clearly dominated by sizeable Dutch–roll oscillations, superimposed over a slow spiral convergence. At the steady state, also in this case, the UAV was significantly banked.

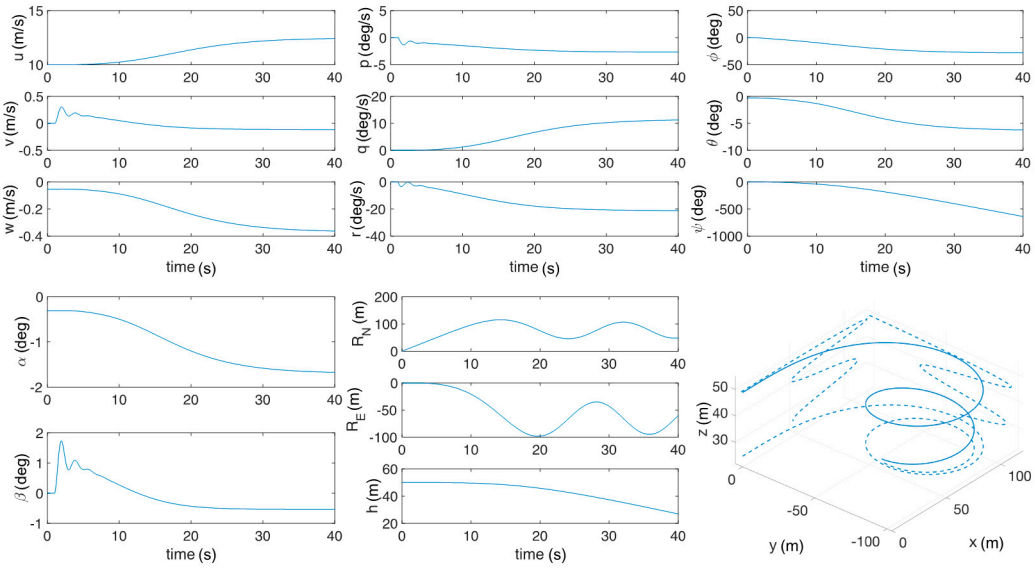

Figure 10. UAV response to the unit step rudder.

3.1.2. Closed-Loop Simulations

Discrete displacements of mobile surfaces give the possibilities of performing a wide range of maneuvers. Simulink was used to develop a stability and control augmentation system suitable for the chosen UAV: the comparison between continuous and discrete commands on closed-loop performance was made. As in [33], a LQR was developed for the virtual model, with full–state feedback on:

- $(\alpha_{DES} - \alpha)$ and $(q_{DES} - q)$, with α_{DES} and q_{DES} equal to α_{TRIM} and to zero respectively, for longitudinal stability;
- $(p_{DES} - p)$ and $(r_{DES} - r)$, with p_{DES} and r_{DES} equal to zero for lateral–directional stability.

The subscript *DES* refers to the target value. The resulting closed-loop behavior for a 3D gust disturbance (duration 30 s in Figure 11) on the desired value of α, q, p and r is presented by the following pictures.

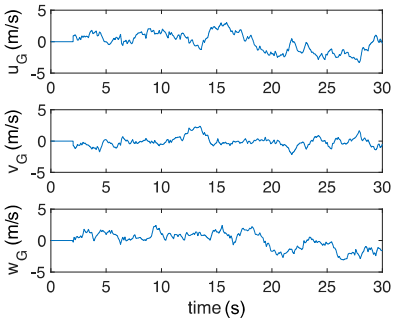

Figure 11. Dryden wind turbulence velocities.

By using a Simulink function, it was possible to implement the Dryden wind turbulence model (continuous) block that uses the Dryden spectral representation to make turbulence acting on the UAV model (in Figure 11 the component velocities of the used Dryden gust were plotted). As it is also possible to see from the figure, the speed components were not correlated with each other and never exceeded ±5 m/s. Since the turbulence in a real scenario was highly dependent on the considered altitude, for the specific case subject of study, the pertinent turbulence model was adopted considering that the evolution of the UAV was enclosed in an altitude range between 45 and 55 m. Another aspect was the turbulence duration: most of the actual gusts lasted a few seconds; in the case of the present investigation a gust lasting about 30 s was used for the simulations representing the worst dynamic scenario. The gust components were incorporated directly into the nonlinear dynamics equations simulating UAV behavior, like perturbations of the aircraft velocity.

The LQ regulator was thus synthesized for the model: the cost functions, previously defined, were associated with the deviations due to the gust perturbation of UAV altitude and attitude from the trim values. The control law developed by LQR obviously does not take into account if the command is continuous or discrete, but simply provides a deflection value of the surface needed for achieving the DES (i.e., desired) conditions. The resulting closed-loop gust response with continuous mobile surfaces is provided by the dotted lines in Figure 12a. In order to satisfy the cost functions, the resulting elevator deflection falls in the range between ±20° (Figure 12a top); the ailerons instead show very low deflections needed to guarantee the desired flight conditions (Figure 12a centre); the rudder must deflect ±10° to maintain the lateral directional stability (Figure 12a bottom). The closed-loop behavior of the conventional LQR controller was acceptable, with minor changes around the trim conditions (these results are not reported in Figure 12b for the sake of clearness of the plot). These results confirm the good stability performance of the chosen UAV.

A control law was then developed for the UAV model operated by discrete commands: ±2° for the elevator and ±0.5° for the ailerons were the discrete limit deflections. The resulting control law is represented by continuous blue lines in Figure 12a where the deflections were evaluated in order

to satisfy the cost functions. In this case the closed-loop behavior was also clearly acceptable (see Figure 12b): the UAV trajectory almost always remained within a 5 m diameter cylinder, centered at the trim trajectory. More in details, in Figure 12b the different trajectory components were reported: z represents the altitude and (x,y) plane was the horizontal plane parallel to the ground. From the Figure 12b it is clear that the vehicle, under the action of the gust and the reaction of the discrete controls, moved around the trim conditions with apparent oscillations that were always confined in about 5 m. To simulate also the actual bistable devices, the piezoelectric MFC actuator was integrated into the Simulink model taking into account its activation law. For the snap transition between the two stable positions of the control plate, it is necessary to send an electric discharge to the MFC actuator. Therefore, a charging time, allegedly affecting the overall dynamics of the system, was added to the control law. The charging time was needed by the condenser for the subsequent discharge generation activating the MFC: the numerical simulations including this charging time (order of 1 s) demonstrated that this aspect was not critical for the control of the vehicle.

The results showed in this section proved that the discrete controller concept was actually working.

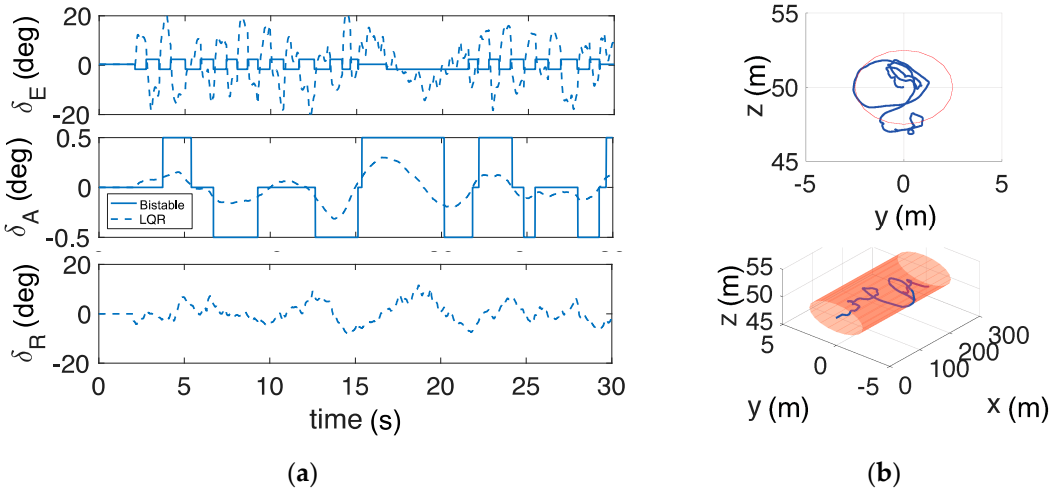

Figure 12. UAV gust response: (**a**) elevator, ailerons and rudder deflections (continuous and discrete behavior) and (**b**) UAV 3D trajectory with discrete command surfaces.

3.1.3. FEM vs. Experimental Plate Results

The numerical FE model was developed (i) to numerically evaluate the plate geometry after the cooling down, (ii) to simulate the plate displacements in order to compare these results with the experiments and (iii) to obtain the maximum cambers with different degrees of application of the "lever effect". FE models furthermore drive the choice of the bistable dimensions and stacking sequence to replace UAV conventional mobile surfaces. A plate 80 mm × 160 mm was simulated by stacking four laminas ($0_2/90_2$) of Hexply 8552 (Hexcel, Stamford, CT, USA). Typical results (deformations) are shown in Figure 13: the numerical maximum cambers are also reported and compared with the experimental results.

The "lever effect" was introduced to constrain the laminate used like an aerodynamic mobile surface (see Figure 14): "S" indicates the distance in mm from the septum position to the bistable constrained edge (in order to better understand the meaning of the symbol "S" used throughout the text, Figure 5 can be looked at). At each value of "S" it is possible to evaluate the maximum deflection of the discrete mobile surface (vertical displacement f, rotation angle).

The airfoil NACA0011, currently used for the stabilizer of the chosen UAV, was virtually integrated with the design bistable plate: the discrete deflections of the bistable plate (a) and of the compliant profile (b) are plotted in Figure 14. Table 3 summarizes the geometric results: these proved that by choosing proper configuration of constraints, lay-up and AR for the bistable plates it is possible to

tailor the snap-through mechanism to make bistables actually operating like mobile surfaces. For each S value, the bistable discrete mobile surface had a deflection angle (in Table 3) comparable with a conventional UAV control surface.

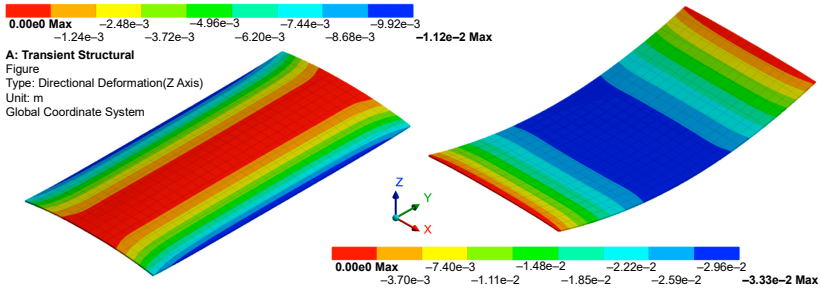

Max camber	Stable state 1	State stable 2
Experimental (mm)	10.5	32.1
FEM (mm)	11.2	33.3
Relative error (%)	6.1	3.7

Figure 13. FE bistable model (two stable state shapes deformations): simulated and measured cambers.

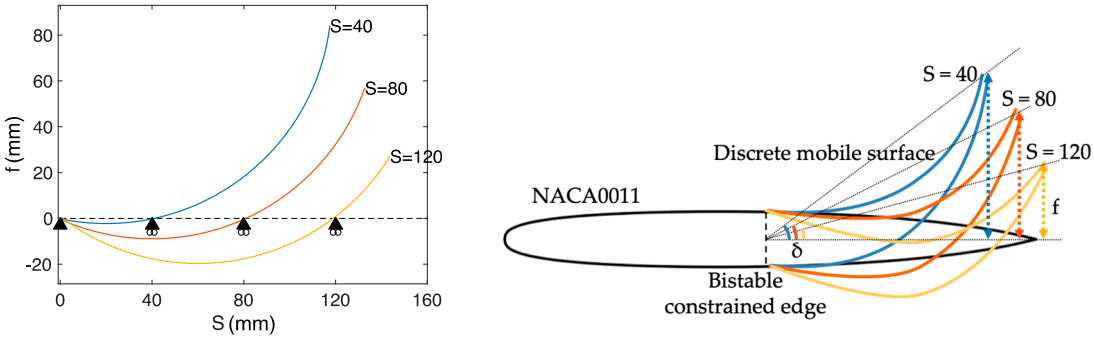

Figure 14. Discrete mobile surface with "lever effect": (**a**) plate deflection f with different value of S; and (**b**) airfoil NACA0011 with different bistable angles δ and deflections f.

Table 3. Deflection f and δ for each values of S.

S (mm)	Deflection f (mm)	Deflection Angle δ (°)
40	84.1	≈28
80	56.9	≈20
120	27.1	≈10

3.2. Wind Tunnel Experiment

The FE simulations showed that, using the "lever effect", the deflection of an aerodynamic surface made of bistable can be comparable with the one of conventional configuration. In order to prove experimentally this idea, a wing sample was made up of balsa, using NACA0011 as a base profile. A bistable plate exploiting the lever effect was integrated in the base profile (Figure 15a). The forward spar was used as clamp for the short side of the plate, while the intermediate support was realized by a mobile septum in order to achieve the lever effect before presented and discussed. In this way the MFC actuator in future developments of this concept will be able to activate the snap-through: each stable state of the composite laminate provided a discrete position of the mobile control surface, due to the compliant skin at the profile trailing edge (Figure 15b).

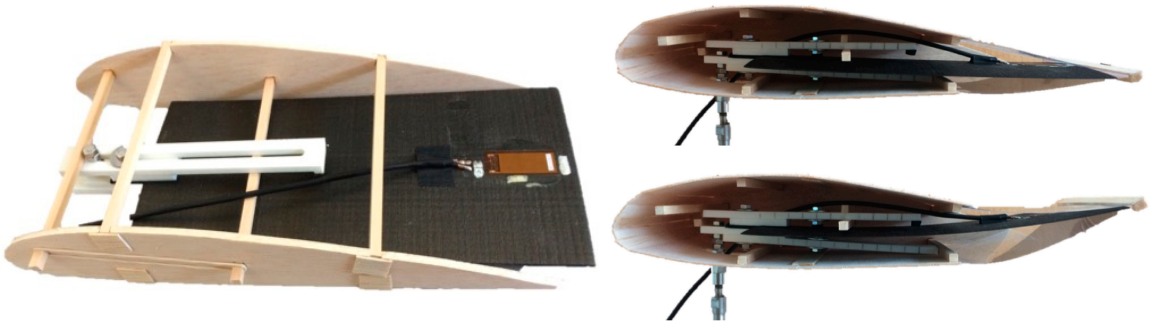

(**a**) (**b**)

Figure 15. Experimental NACA 0011 airfoil (**a**) sample without the skin and (**b**) discrete mobile surface OFF (top) and ON (bottom).

The capability of the wing sample to keep the shapes at several flight speeds and at different AOAs was evaluated by carrying out specific tests represented in Figure 16.

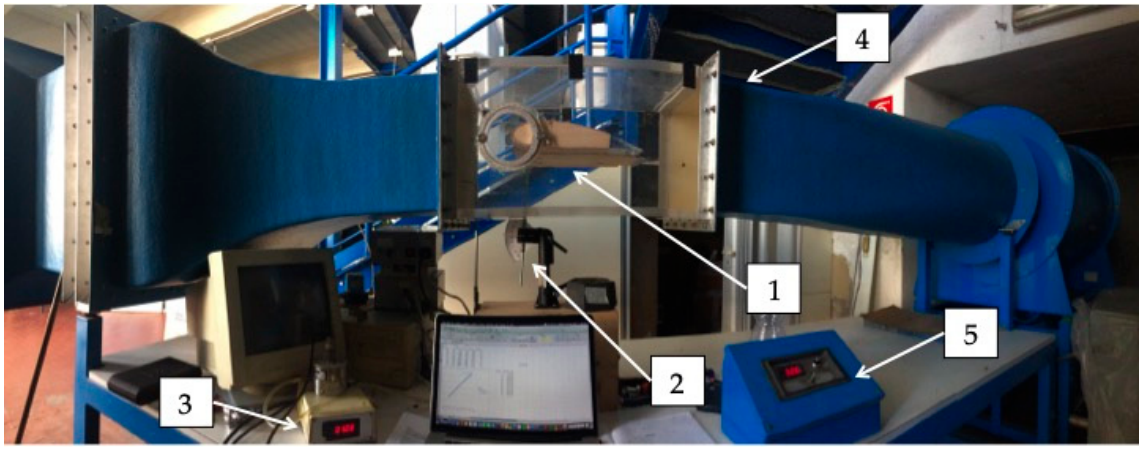

(**a**)

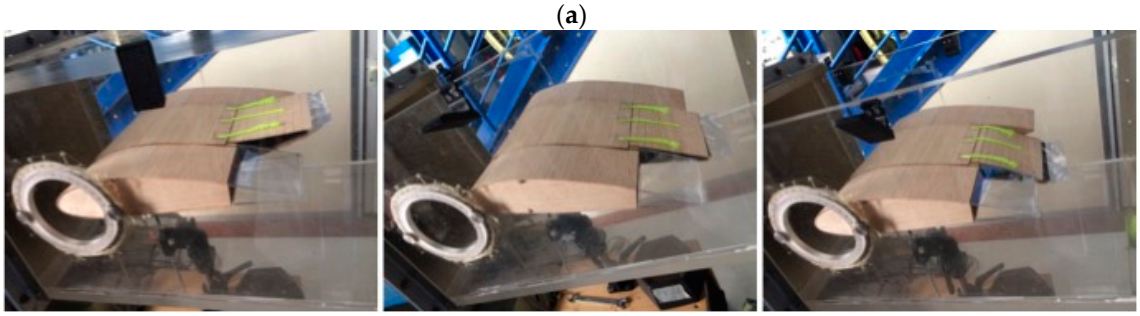

(**b**)

Figure 16. Wind tunnel experiment: (**a**) 1. Sample profile with discrete mobile surface, 2. angles of attack (AOA) tool (min −15°, max +20°), 3. pitot tube, 4. test chamber and 5. wind speed regulator and (**b**) negative (LEFT), neutral (CENTRE) and positive (RIGHT) deflection of discrete mobile surface.

The scope of the aerodynamic campaign was to demonstrate the stability of every state of the mobile surface when operating in an external field. In this context stability of an initial state means that, following a small perturbation of the external flow (i.e., caused by a local separation of the flow around the profile or by the turbulence), the bistable keeps its geometric shape without snapping to the other shape. The possible bistable initial states were four, two for each stable state (see Figure 17, where it is clear that the plate can be installed in one specific geometric configuration and the corresponding reverse one, UP and DOWN respectively). During the experimental tests the external field was accelerated at different AOAs waiting for a "natural" snap through, i.e., not activated by any sensor

(MFC). This campaign was extremely useful for understanding if the mobile surface can be prone to unwanted deflection.

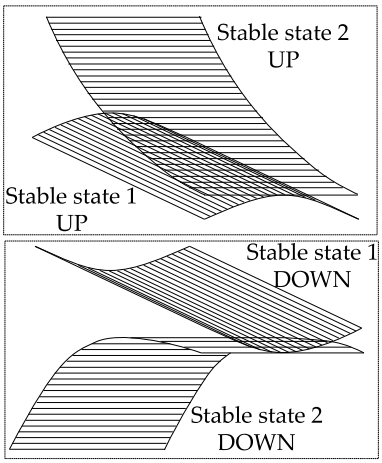

Figure 17. Bistable plates configurations.

An accurate aerodynamic experimental campaign was carried out in a wind tunnel of the type "open circuit". *S* was equal to 80 mm, to which corresponds a deflection angle of about 20°, as it can be seen in Table 3. Two different sample configurations were tested, according to the scheme in Figure 17, to allow the study (varying AOA and flight speed) of the snap behavior, due to the aerodynamic load, for positive and negative deflections of the mobile surface. Table 4 lists the speeds at which the snap through occurred: the stable state 1 (in both the configurations) was the most suitable to withstand the aerodynamic external pressure, whereas the stable state 2—UP configuration suffered negative AOAs and the stable state 2—DOWN configuration suffered positive AOAs, i.e., snapping without external activation. This result was consistent with the static characterization of the bistable plates reported in [15] where it is experimentally shown that the stable state 1 is stiffer (i.e., requires more energy for the transition to the other state) than stable state 2.

Table 4. Experimental wind tunnel results.

AOA (°)	Initial Stable State			
	1—UP	**2—UP**	**1—DOWN**	**2—DOWN**
	Snap Speed (km/h)			
+20	85	-	-	35
+15	-	-	-	45
+10	-	-	-	50
+5	-	-	-	65
0	-	60	-	70
−5	-	70	-	-
−10	-	55	-	-
−15	-	45	-	-

In conclusion, the proposed morphing concept passed the wind tunnel test, showing significant aerodynamic withstanding at AOAs and flight speeds that are typical of the size of the employed UAV. These results also suggested a solution to replace the conventional UAV stabilizer (with weight around 0.5 kg) with an innovative horizontal tail with discrete bistable elevators (see CAD in Figure 18a). The proposed concept appeared lighter (bistable plates and lever effect tool weigh around 0.3 kg) and increased aerodynamic efficiency (without any servomechanism outside of the tail airfoil) when compared to conventional UAV command surfaces.

Four bistable plates (in Figure 18a) could be installed on a modified leading edge of the new horizontal tail with the lever effect tool integrated (Figure 18b): a pair of plates could be installed in the UP configuration, and a pair of plates could be installed in the DOWN configuration (see Figure 17). In this way when they are not activated, their first stable shape provides the neutral position of the stabilizer; when one pair is activated it is possible to achieve a deflection of the stabilizer upwards/downwards depending on which one of the two pairs (UP/DOWN respectively) is activated.

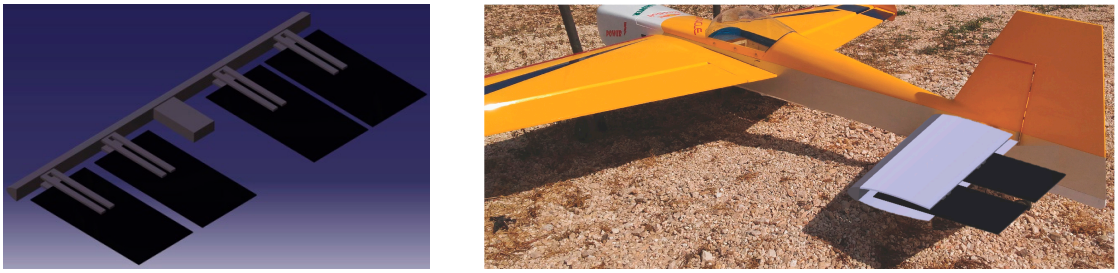

(**a**) (**b**)

Figure 18. New horizontal tail concept: (**a**) bistable horizontal tail in CATIA and (**b**) UAV equipped with the concept of a horizontal bistable stabilizer.

3.3. Takeoff Length: Numerical vs. Experimental Results

This final subsection summarizes the results of three experimental tests and Simulink simulations related to the UAV take-off length. The experimental campaign was carried out with the conventional UAV stabilizer operating in "discrete" mode (just two possible deflections): this choice of using the convectional stabilizer and not the bistable one was motivated by the circumstance that, in the event of failure or an unwanted dynamic evolution of the UAV, the conventional commands would have allowed a prompt and full recovery of the UAV. As suggested by the RC UAV manufacturer, during the maneuver and the Simulink simulations, the engine throttle underwent a gradual increase up to 60% of the maximum in 10 s for the take-off maneuver. In the following pictures, white-red reference elements were placed at a distance of 5 m from each other.

The first take-off test was carried out assuming the stabilizer deflection equal to −10°; this deflection was constant from the beginning of the test until the UAV took off from the ground: the vehicle was soared in flight after having covered 18.7 m of runway in 4 s (Figure 19).

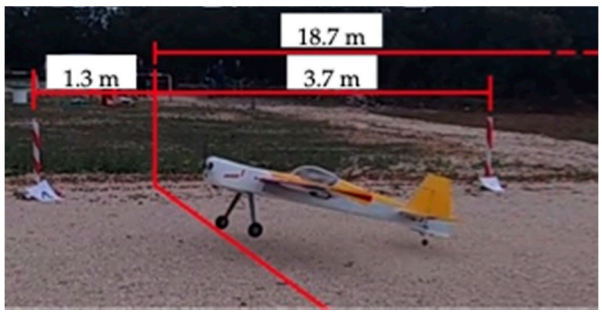

Figure 19. Runway length at first takeoff time.

The second take-off test was carried out assuming the stabilizer deflection equal to 0°; this deflection was constant: the UAV was not able to take-off using the whole runway length of 35 m. The last take-off test was performed like a traditional maneuver: taxing with the stabilizer in neutral position until 3 s, and subsequent −10° deflection on the horizontal tail command. Under these conditions, the UAV was able to lift off after 12.5 m of runway, in 3.5 s.

Table 5 reports the numerical results obtained Simulink in which the motion equations were solved and the experimental results.

Table 5. Take-off results.

Test		Results	Experimental	Simulink	Error (%)
1	$\delta_E = -10°$	Runway (m)	18.7	17.6	5.9
		Time (s)	4	3.8	5.0
2	$\delta_E = 0°$	Runway (m)	35	35	-
		Time (s)	6	5.7	5.0
3	0–3 s, $\delta_E = 0°$ from 3 s on, $\delta_E = -10°$	Runway (m)	12.5	13.6	−8.8
		Time (s)	3.5	3.2	5.7

The errors on time and space were so explained:

- Ground friction coefficient: in Simulink simulations this was constant, in actual tests the runway was definitely uneven and not properly described by a constant friction coefficient;
- Measurement time: the error of human reaction was about three tenths of a second;
- Wind: the actual weather was quickly changing, with small gusts from different directions, while no gust model was included in the Simulink code;
- UAV weight distribution: it was assumed homogeneous in the Simulink model for sake of simplicity, and at this stage of the research this small error can be accepted;
- Ground effect: it was not included in the Simulink model.

In conclusion, the Simulink code was able to predict the UAV behavior, either during taxing and flight maneuver, either with conventional and discrete mobile control surfaces. Now it can be stated that the proposed innovative concept of bistable morphing control surfaces on a RC-UAV can go to the next research step: implementation of the actual prototype of new UAV horizontal stabilizer, by using composite bistable plates integrated with the lever effect tool due to the data gathered during this research phase.

4. Conclusions

In this study a new horizontal stabilizer was presented for RC-UAV application, by using composite bistable laminates. The nonlinear flight dynamics equations were implemented in Simulink to study different flight conditions. These numerical results were used as inputs to the FE model of bistable composite plates. By using the "lever effect", it was demonstrated that the shapes of the bistable plates could be tailored to mimic the conventional command surfaces behavior. Composite bistable plates were built with AR, dimensions, asymmetric stacking sequence and total thickness, previously simulated. The new bistable elevator was tested in the wind tunnel and the discrete mobile surface behavior was validated through real flight tests, carried out using a actual RC-UAV. The present manuscript just reports a preliminary investigation on the technical feasibility of a control surface based on the employment of bistable materials. Basic research questions aimed at proving that the concept could actually work were addressed positively. Future work will be based on a robust design of the control surface consisting in the optimization of the aerodynamic efficiency of the surface, through numerical and wind-tunnel tests, and in a proper evaluation of the energy required for the operation of the control. After all the design stages will be completed, a prototype of bistable horizontal stabilizer, activated by a MFC actuator, will be installed on a UAV and flight tested.

Author Contributions: Conceptualization, G.S.; methodology, G.S. and F.N.; software, F.N.; validation, G.S. and F.N.; formal analysis, G.S.; investigation, F.N.; resources, G.S.; data curation, F.N.; writing—original draft preparation, F.N.; writing—review and editing, G.S.; visualization, G.S. and F.N.; supervision, G.S.; project administration, G.S.

Funding: This research received no external funding.

Acknowledgments: All the authors are grateful to Giuseppe Del Core (Uniparthenope) and Giulio Avanzini (Unisalento) for their kind scientific suggestions and they acknowledge the thesis work done by Giammario Ferrara, who helped them in testing the actual UAV with discrete mobile surface.

Conflicts of Interest: The authors declare no conflict of interest.

References

1. Dalamagkidis, K. Definitions and terminology. In *Handbook of Unmanned Aerial Vehicles*; Springer: Dordrecht, The Netherlands, 2015; pp. 43–55. ISBN 9789048197071.
2. Valavanis, K.P. Introduction. In *Advances in Unmanned Aerial Vehicles: State of the Art and the Road to Autonomy*; Springer: Berlin/Heidelberg, Germany, 2007; Volume 33, ISBN 978-1-4020-6113-4.
3. Zeng, Y.; Zhang, R.; Lim, T.J. Wireless communications with unmanned aerial vehicles: Opportunities and challenges. *IEEE Commun. Mag.* **2016**, *54*, 36–42. [CrossRef]
4. Saad, W.; Mozaffari, M.; Yin, C.; Hong, C.S.; Chen, M.; Debbah, M. Caching in the Sky: Proactive Deployment of Cache-Enabled Unmanned Aerial Vehicles for Optimized Quality-of-Experience. *IEEE J. Sel. Areas Commun.* **2017**, *35*, 1046–1061.
5. Hodgson, J.C.; Koh, L.P. Best practice for minimising unmanned aerial vehicle disturbance to wildlife in biological field research. *Curr. Biol.* **2016**. [CrossRef] [PubMed]
6. Anderson, K.; Gaston, K.J. Lightweight unmanned aerial vehicles will revolutionize spatial ecology. *Front. Ecol. Environ.* **2013**, *11*, 138–146. [CrossRef]
7. Cano, E.; Horton, R.; Liljegren, C.; Bulanon, D. Comparison of Small Unmanned Aerial Vehicles Performance Using Image Processing. *J. Imaging* **2017**. [CrossRef]
8. Balek, J.; Blahůt, J. A critical evaluation of the use of an inexpensive camera mounted on a recreational unmanned aerial vehicle as a tool for landslide research. *Landslides* **2017**. [CrossRef]
9. Battipede, M.; Vazzola, M.; Tancredi, D. Innovative Piloting Technique for a Semi-Autonomous UAV Lighter-Than-Air Platform Simulator. In *Proceedings of the AIAA Modeling and Simulation Technologies Conference*; American Institute of Aeronautics and Astronautics: Reston, VI, USA, 2012.
10. Hosseini, S.; Mesbahi, M. Energy-Aware Aerial Surveillance for a Long-Endurance Solar-Powered Unmanned Aerial Vehicles. *J. Guid. Control Dyn.* **2016**, *39*, 1980–1993. [CrossRef]
11. Panagiotou, P.; Kaparos, P.; Salpingidou, C.; Yakinthos, K. Aerodynamic design of a MALE UAV. *Aerosp. Sci. Technol.* **2016**, *50*, 127–138. [CrossRef]
12. Panagiotou, P.; Giannakis, E.; Savaidis, G.; Yakinthos, K. Aerodynamic and structural design for the development of a MALE UAV. *Aircr. Eng. Aerosp. Technol.* **2018**, *90*, 1077–1087. [CrossRef]
13. Sharma, R.; Panigrahi, R.K. Stokes based sigma filter for despeckling of compact PolSAR data. *IET Radar Sonar Navig.* **2018**, *12*, 475–483. [CrossRef]
14. Kontogiannis, S.G.; Ekaterinaris, J.A. Design, performance evaluation and optimization of a UAV. *Aerosp. Sci. Technol.* **2013**, *29*, 339–350. [CrossRef]
15. Nicassio, F.; Scarselli, G.; Pinto, F.; Ciampa, F.; Iervolino, O.; Meo, M. Low energy actuation technique of bistable composites for aircraft morphing. *Aerosp. Sci. Technol.* **2018**, *75*, 35–46. [CrossRef]
16. Scarselli, G.; Maffezzoli, A.; Nicassio, F. Mechanical characterization of bistable laminates for very small aircraft morphing applications. In Proceedings of the Health Monitoring of Structural and Biological Systems XII, Denver, CO, USA, 4–8 March 2018; p. 61.
17. De Breuker, R.; Werter, N. On the Importance of Morphing Deformation Scheduling for Actuation Force and Energy. *Aerospace* **2016**, *3*, 41. [CrossRef]
18. Arena, M.; Nagel, C.; Pecora, R.; Schorsch, O.; Concilio, A.; Dimino, I. Static and Dynamic Performance of a Morphing Trailing Edge Concept with High-Damping Elastomeric Skin. *Aerospace* **2019**, *6*, 22. [CrossRef]
19. Sofla, A.Y.N.; Meguid, S.A.; Tan, K.T.; Yeo, W.K. Shape morphing of aircraft wing: Status and challenges. *Mater. Des.* **2010**, *31*, 1284–1292. [CrossRef]
20. Pecora, R.; Barbarino, S.; Concilio, A.; Lecce, L.; Russo, S. Design and functional test of a morphing high-lift device for a regional aircraft. *J. Intell. Mater. Syst. Struct.* **2011**, *22*, 1005–1023. [CrossRef]
21. Della Vecchia, P.; Corcione, S.; Pecora, R.; Nicolosi, F.; Dimino, I.; Concilio, A. Design and integration sensitivity of a morphing trailing edge on a reference airfoil: The effect on high-altitude long-endurance aircraft performance. *J. Intell. Mater. Syst. Struct.* **2017**, *28*, 2933–2946. [CrossRef]
22. Nicassio, F.; Scarselli, G.; Avanzini, G.; Del Core, G. Numerical and experimental study of bistable plates for morphing structures. In Proceedings of the Active and Passive Smart Structures and Integrated Systems 2017, Portland, OR, USA, 25–29 March 2017; p. 101640K.

23. Kim, S.W.; Lee, J.Y.; Cho, K.J. Towards a bistable morphing winglet for unmanned aerial vehicle (UAV). In Proceedings of the 2013 44th International Symposium on Robotics, Seoul, Korea, 24–26 October 2013; pp. 1–3.
24. Mills, J.; Ajaj, R. Flight Dynamics and Control Using Folding Wingtips: An Experimental Study. *Aerospace* **2017**, *4*, 19. [CrossRef]
25. Wang, B.; Fancey, K.S. A bistable morphing composite using viscoelastically generated prestress. *Mater. Lett.* **2015**, *158*, 108–110. [CrossRef]
26. Tawfik, S.A.; Stefan Dancila, D.; Armanios, E. Unsymmetric composite laminates morphing via piezoelectric actuators. *Compos. Part A Appl. Sci. Manuf.* **2011**, *42*, 748–756. [CrossRef]
27. Soken, H.E.; Ersin Soken, H.; Yenal Vural, S.; Hajiyev, C.; Vural, S.Y. Equations of Motion for an Unmanned Aerial Vehicle. In *State Estimation and Control for Low-cost Unmanned Aerial Vehicles*; Springer International Publishing: Cham, Switzerland, 2015; pp. 9–23.
28. XFOIL Subsonic Airfoil Development System. Available online: http://web.mit.edu/drela/Public/web/xfoil (accessed on 6 March 2019).
29. Scarselli, G.; Nicassio, F.; Pinto, F.; Ciampa, F.; Iervolino, O.; Meo, M. A novel bistable energy harvesting concept. *Smart Mater. Struct.* **2016**. [CrossRef]
30. ANSYS Product Launcher. Available online: https://ansyshelp.ansys.com (accessed on 6 March 2019).
31. Hexcel Prepreg. Available online: https://www.hexcel.com/Resources/DataSheets/Prepreg (accessed on 6 March 2019).
32. MACRO FIBER COMPOSITE–Smart-Material. Available online: https://www.smart-material.com/Datasheets-MFC.html (accessed on 6 March 2019).
33. Avanzini, G.; Nicassio, F.; Scarselli, G. Reduced-Order Short-Period Model of Flexible Aircraft. *J. Guid. Control Dyn.* **2017**, *40*, 2017–2029. [CrossRef]